THE ASTRONOMICAL JOURNAL VOLUME 113, NUMBER 6 JUNE 1997

TWO-COLOR SURFACE PHOTOMETRY OF BRIGHTEST CLUSTER MEMBERS

BIANCA GARILLI, GIORGIO SANGALLI, STEFANO ANDREON,[1] AND DARIO MACCAGNI

Istituto di Fisica Cosmica del CNR, via Bassini 15, 20133 Milano, Italy
Electronic mail: bianca,sangalli,andreon,dario@ifctr.mi.cnr.it

LUIS CARRASCO[2] AND ELSA RECILLAS[2]

Instituto Nacional de Astrofisica Óptica y Electrónica, Apartado Postal 51 y 216, 72000 Puebla, Pue., Mexico
Electronic mail: carrasco,elsare@tonali.inaoep.mx

Received 1996 July 31; revised 1997 January 17

ABSTRACT

The Gunn g, r, and i CCD images of a representative sample of 17 Brightest Cluster Galaxies (BCM) have been analyzed in order to derive surface brightness and color profiles, together with geometrical parameters like eccentricity and position angle. The sample includes both X-ray and optically selected clusters, ranging in redshift from $z=0.049$ to $z=0.191$. We find that BCMs are substantially well described by de Vaucouleurs' law out to radii of $\sim 60-80$ kpc, and that color gradients are generally absent. Only in two cases we find a surface brightness excess with respect to the $r^{1/4}$ law, which for A150 is coupled with a change in the $g-r$ color. The rest frame colors of BCMs do not show any intrinsic dispersion. By parametrizing the environment with the local galaxy number density, we find that it is correlated with the BCM extension, i.e., BCMs with larger effective radii are found in denser environments. © *1997 American Astronomical Society.* [S0004-6256(97)00105-2]

1. INTRODUCTION

For many galaxies, the cluster environment is considered hostile, often leading to interactions bound to modify their structure and perturbing the quiet deployment of their properties. This is at least what is happening *now*, what we observe in the dense cluster environments at the present epoch in the form of perturbed morphologies. However, the cluster environment has also had a great success in favoring the formation of massive galaxies, specifically the most luminous galaxies that are found. How has this occurred, and when? And what is the relation of these brightest cluster galaxies with the surrounding cluster members, the cluster morphology, and the density of the hot intracluster gas?

The study of brightest cluster members and of their structural parameters has been traditionally pursued. The better visibility of these objects has made them useful cosmological tools, similar to supernovae in certain aspects. In order to use them as standard candles, their properties have to be understood, and their possible differences studied in terms of induced potential biases due to similar yet somewhat different environments. This line of research is still being followed, and would be further complemented by an investigation of the properties of these giant galaxies aimed at understanding their process of formation and evolutionary status.

We have recently completed a photometric survey of the cores of clusters of galaxies selected both through their X-ray emission properties and optically through the density contrast over the field (Garilli *et al.* 1996, from now on Gar96). In that paper it was shown that the same kind of passive evolution is shared by the whole early type galaxy population in a cluster, and no difference is evident between clusters selected in either way. In this paper, we analyze the data set of Gar96 in an attempt to infer the structural properties for a subsample of brightest cluster members (BCM), and we try to demonstrate that there is a correlation between the size of the BCM and the *local* galaxy density within the cluster, as Andreon *et al.* (1992, 1995) had suggested from a study of a much smaller sample.

This paper is organized in the following way: in Sec. 2, we describe the sample and the analysis tools; in Sec. 3, we present the properties of the studied galaxies, specifically their isophotal shapes, their surface brightness profiles and color profiles; in Sec. 4, we discuss the inferred BCM properties in relation to some other cluster observable parameters.

Throughout this paper we adopt $H_0=50$ km s^{-1} Mpc^{-1} and $q_0=0.5$.

2. THE DATA

2.1 The Sample

The number of BCMs free from large superposed objects and for which our data allow a surface brightness analysis out to a reasonable radius is 17, out of the 67 clusters for which g, r, and i photometry had been secured from the 2.1 m telescope of the *Observatorio Astronomico Nacional* in San Pedro Martir, Mexico. Details of the observations are given in Gar96. Table 1 lists the clusters in which the BCMs are found, together with their redshifts, the Bautz–Morgan type (Bautz & Morgan 1970) and the richness class. Clusters marked "blue" or "red" are clusters in which the early type

[1]Present address: Osservatorio Astronomico di Capodimonte, Napoli, Italy.
[2]Also Instituto de Astronomia, UNAM, Mexico D.F., Mexico.

 0004-6256/97/113(6)/1973/10/$10.00

TABLE 1. Cluster characteristics.

Cluster id	redshift z	Bautz–Morgan Type	Richness Class	Notes
MS0002+1556	0.116	...	...	...
MS0013+1558	0.083	...	...	...
MS0037+2917 (A77)	0.072	I	1	...
A84	0.103	II	1	...
MS0102+3255	0.080	...	...	...
A150	0.060	I–II	1	...
A180	0.135	I	0	blue
A279	0.080	I–II	1	...
A399	0.072	I–II	1	...
A401	0.075	I	2	...
MS0301+1516	0.083	...	...	red
A671	0.049	II–III	0	...
A733	0.116	I	1	...
MS0904+1651 (A744)	0.073	II	1	blue
MS1201+2824	0.167	...	...	...
A1911	0.191	II–III	2	...
MS1558+3321 (A2145)	0.088	...	0	...

galaxy sequence is either significantly bluer or redder than what expected from a properly normalized Virgo color–magnitude relation (see Gar96). These clusters could have followed an evolution slightly different from the one of the bulk of the clusters we studied.

The BCM subsample spans almost the full redshift range of the cluster sample, z ranging from 0.049 to 0.191, it includes 8 X-ray selected and 12 Abell clusters (Abell *et al.* 1989) [3 clusters being included both in the Abell catalog and in the EMSS (Gioia *et al.* 1990) catalog], with B–M type I, I–II, II, and II–III and richness class from 0 to 2. However, if we can claim that our sample spans a vast range of cluster properties, we cannot say that we have an unbiased sample. Our selection of objects favors galaxies with large apparent radii. It is worth mentioning that the selection criteria of the main cluster sample did not consider in any way the presence of a BCM of certain characteristics, nor were the observations specifically tailored to study their surface brightness properties.

2.2 Data Analysis

The 51 images containing the 17 BCMs were reduced and flux calibrated as described in Gar96. Surface photometry, color profiles and structural parameters have been obtained following the procedures described in Andreon *et al.* (1995).

Briefly, the *sky background* has been determined in each image by averaging the count rates in independent areas of 20×20 pixels free from detectable objects and as distant as possible from the BCM. We further required that the growth curves of each BCM actually reached saturation once assumed a sky background level. *Superposed or nearby objects* have been removed and substituted with the interpolated value from nearby pixels prior to any further analysis. In some cases the areas occupied by these objects have been masked. It must be said than in any case these removed objects are faint and small compared with the BCMs. It is worth recalling that the absence of bright superposed objects was one of the selection criteria for our subsample. *Eccentricities and position angles* were computed by means of the STSDAS package in IRAF. In order to keep the S/N ratio approximately constant as the radius increases, we ran the procedures several times over the same images rebinned by a proper factor. *Seeing effects* were considered and the structural parameters have been determined only by taking into account data points outside an aperture 4 times the FWHM of the seeing disc. The average seeing during our observations was $\sim2''$. We have obtained the *eccentricity and position angle* profiles outside the region affected by seeing and used intensity weighted averages and center coordinates determined by STSDAS to compute the *surface brightness profiles*. These profiles were obtained by integration of the counts in elliptical coronae of fixed eccentricity and position angle and of a step variable according to S/N criteria. From the surface brightness profiles in the three filters, *color profiles* have been extracted and analyzed with respect to possible color gradients following the method described by Sparks & Jørgensen (1993) and further developed by Andreon *et al.* (1995).

3. RESULTS

3.1 Isophote Fitting, Eccentricity, and Position Angle

Ellipses are an excellent fit to the isophotes of every BCM studied here, as implied by their a_n Fourier coefficients that do not deviate from 0 in any significant manner. However, only effects larger than 5% could be detected in our data.

For all galaxies in our sample, the eccentricity and position angle profiles do not significantly differ in the three filters. Figure 1 shows the eccentricity and position angle plots as a function of the logarithm of the major axis expressed in kpc. In Table 2, for each BCM (column 1), we give the minimum and maximum radius in kpc over which these parameters have been computed (column 2), an intensity weighted value of the eccentricity $\epsilon=(1-b/a)$ (column 3) and its rate of variation along the radius expressed as $\Delta\epsilon$ kpc^{-1} (column 4), an intensity weighted value of the position angle θ in degrees measured clockwise from the E–W direction (column 5) and its rate of variation along the

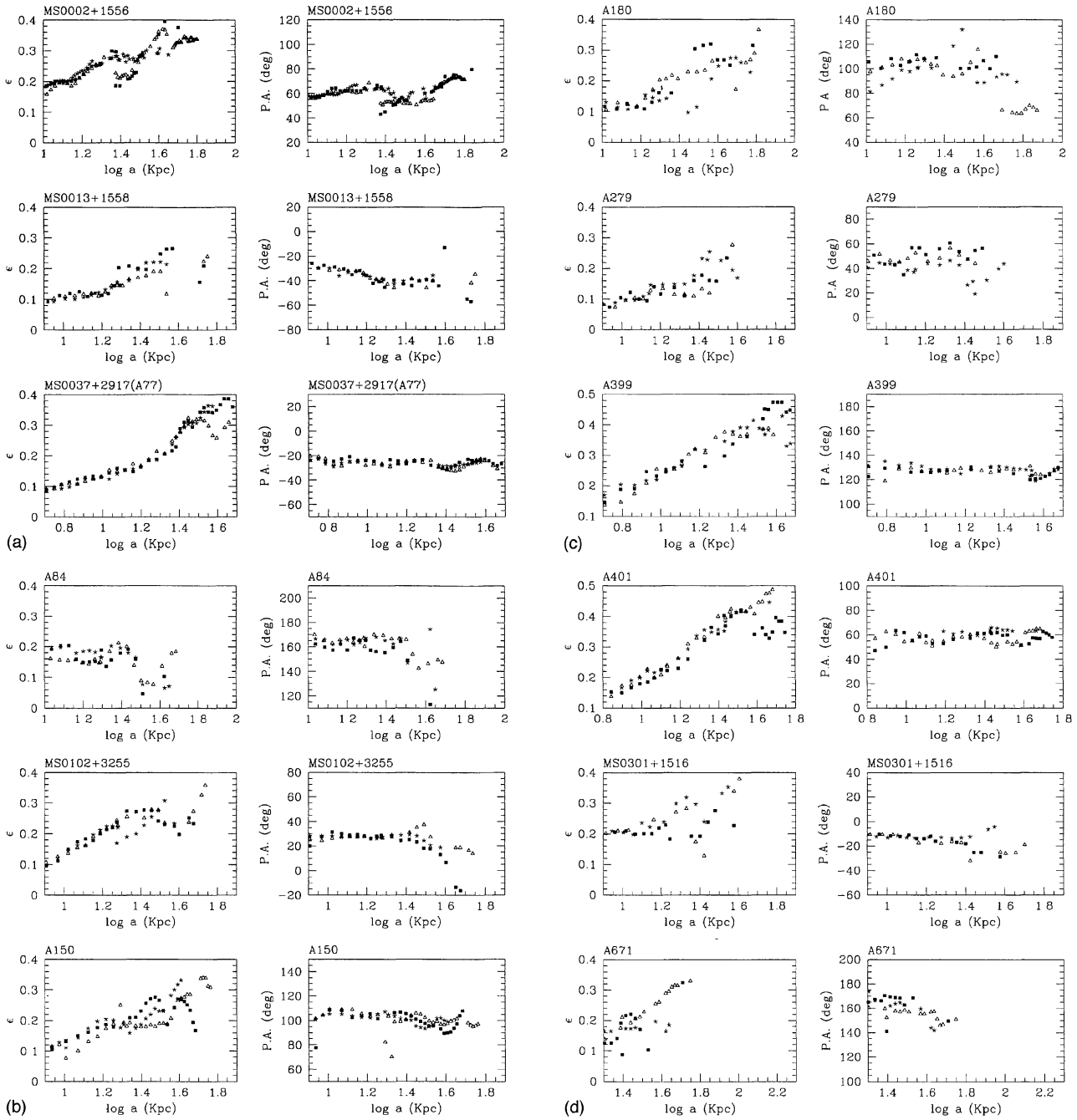

FIG. 1. BCM eccentricity $\epsilon=(1-b/a)$ and position angle P.A. as a function of the logarithm of the semi–major axis a expressed in kpc. *Open triangles*: g band; *full squares*: r band; *stars*: i band.

radius, also expressed as $\Delta\theta$ kpc^{-1} (column 6).

As one can notice, the eccentricities are never larger than 0.3, except in MS1558+3321 (A2145), for which $\epsilon=0.5$. Only in the cases of MS0102+3255, A401, and MS1558 +3321 (A2145) the eccentricity increases rapidly with the radius. The isophotes are concentric within 0.6″, which is the precision limit that can be achieved with our data. The rule is also to have a constant position angle of the isophotes, except in the case of MS0013+1558 for which we detect a change.

3.2 Surface Brightness Profiles

In Fig. 2 we present the BCM rest–frame surface brightness profiles in the r bandpass plotted as function of $r^{1/4}$. At small radii our data are affected by seeing effects and consequently for those central regions the following arguments do not apply. At large radii we are limited by our flat-fielding and S/N ratios. The arrows in the plots indicate the galaxy rest frame surface brightness at a level 5 magnitudes fainter than the sky background. In the case of A401 our profile stops before this surface brightness limit as the edge

TABLE 2. BCM eccentricities and position angles.

Cluster id	$a_{min}-a_{max}$ kpc	ϵ	$\Delta\epsilon$ kpc^{-1}	θ degrees	$\Delta\theta$ kpc^{-1}
MS0002+1556	17–65	0.30	0.003	65	0.6
MS0013+1558	10–58	0.20	0.006	−38	1.2
MS0037+2917 (A77)	9–49	0.20	0.008	−26	···
A84	13–41	0.18	···	165	···
MS0102+3255	10–47	0.23	0.012	28	···
A150	9–49	0.18	0.008	105	···
A180	16–44	0.22	0.005	103	···
A279	12–30	0.13	0.007	46	···
A399	7–51	0.27	0.006	128	···
A401	8–55	0.29	0.010	59	···
MS0301+1516	12–37	0.26	0.003	−14	···
A671	4–36	0.19	0.005	157	···
A733	6–41	0.11	···	265	0.8
MS0904+1651 (A744)	9–43	0.06	···	185	···
MS1201+2824	22–44	0.30	···	95	0.4
A1911	22–41	0.30	0.001	76	0.3
MS1558+3321 (A2145)	11–61	0.50	0.013	82	···

of the CCD image was reached. The structural parameters have been derived considering only those portions of the profiles, while, whenever meaningful, the profiles themselves have been extended to fainter surface brightnesses in order to investigate the possible presence of extended halos.

For each galaxy in Fig. 2 we also show as a continuous line the best fitting de Vaucouleurs' law (de Vaucouleurs 1948). In the fitting procedure, only those data points that can be considered statistically independent given the image seeing have been taken into account. For each BCM, we report in Table 3 the results of the fits to the $r^{1/4}$ law. In column 2 and 3 we give the effective radius r_e in kpc and the effective surface brightness μ_e in r mag arcsec^{-2}, respectively. The quoted errors represent the 90% confidence levels given by the fitting procedure. The surface brightness magnitudes were corrected for k-dimming, galactic absorption, and atmospheric extinction following Schneider *et al.* (1983a) and Stark *et al.* (1992), and also corrected for the $(1+z)^4$ cosmological dimming. Column 4 lists the obtained reduced χ^2. Column 5 and 6 give the rest–frame mean $g-r$ and $r-i$ colors, and column 7 the absolute magnitude M_r computed within the 38 kpc radius. Generally, the de Vaucouleurs' law provides a satisfactory fit. We do not think that our data justify any fit with a different, more generalized law like the $r^{1/n}$ proposed by Sersic (1968) and recently adopted by Caon *et al.* (1993) and Graham *et al.* (1996).

From the radial light profiles presented in Fig. 2, we can divide the sample BCMs into three categories: (a) galaxies substantially well described by de Vaucouleurs' law over the whole range of data points; (b) galaxies showing what can be termed a tidal cutoff; and (c) galaxies showing a brightness excess over de Vaucouleurs' law. We would place in category (a) (which we will not further discuss) MS0002+1556, MS0013+1558, MS0102+3255, A180, A401, MS0301+1516, A671, A733, and A1911. MS0037+2917(A77), A279, A399, MS1201+2824, and MS1558+3321(A2145) fall into category (b), and finally, A84, A150, and MS0904+1651(A744) are good candidates for the presence of an extended halo (category (c)).

3.2.1 Tidal cutoffs

The profile of MS0037+2917 (A77) mimicks a tidal cutoff beyond ~45 kpc. The apparent size of this galaxy is rather large with respect to the CCD field of view and another bright S0 galaxy is present South of the BCMs. Therefore, there is the possibility that the curvature in the profile (in any case, within 1σ of the de Vaucouleurs' profile) might be due to an overestimate of the sky background rather than to a real physical effect. In A279, a tidal cutoff could be present outward of ~60 kpc at a very low significance level. Furthermore, this occurs beyond the radius where systematic errors are important. Similarly to A77, A399 shows a surface brightness deficit at large radii. Again, because of the large apparent size of this galaxy with respect to the CCD size and of a removed object along the galaxy major axis, we cannot confidently state that this deviation from de Vaucouleurs' law is evidence of a tidal cutoff.

In the case of MS1201+2824, the impression of a surface brightness deficit at large radii is probably due to the somewhat anomalous behavior of the light profile with respect to the de Vaucouleurs' law.

As for MS1558+3321 (A2145), the situation is similar to that of A77 and A399, yet with even less statistical significance.

3.2.2 Extended halos

Of the three BCMs showing some evidence of an extended halo, A84 and MS0904+1651 (A744) show only scanty statistical significance (the extrapolation of the best fit with de Vaucouleurs' law falls within the 1σ error bars of the data points) even if for A744 we were unable to trace the light profile in the rest–frame to a magnitude fainter than $\mu_r \sim 25$ mag arcsec^{-2}.

The case of A150 is different, since this is also the most peculiar BCM in our sample. The light profile shows a sta-

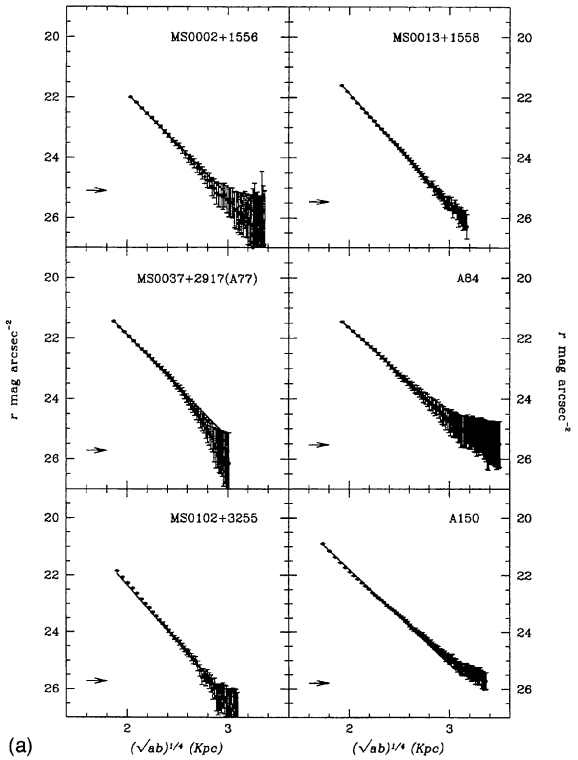

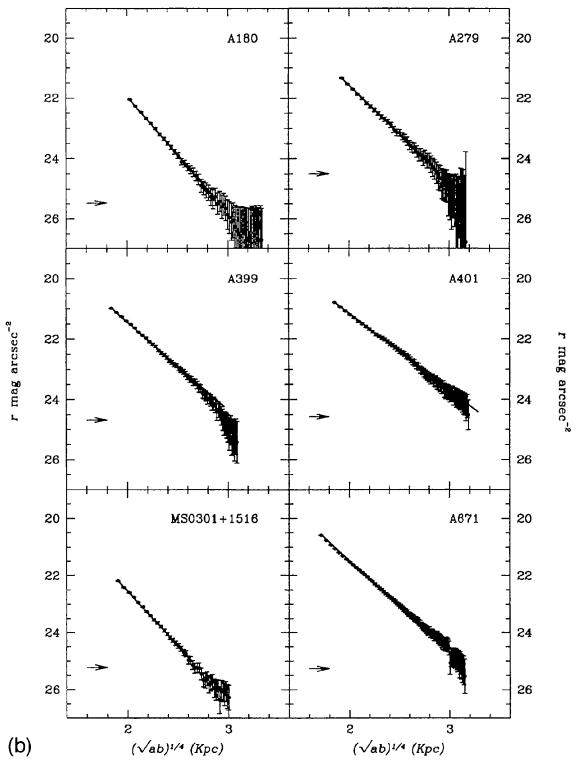

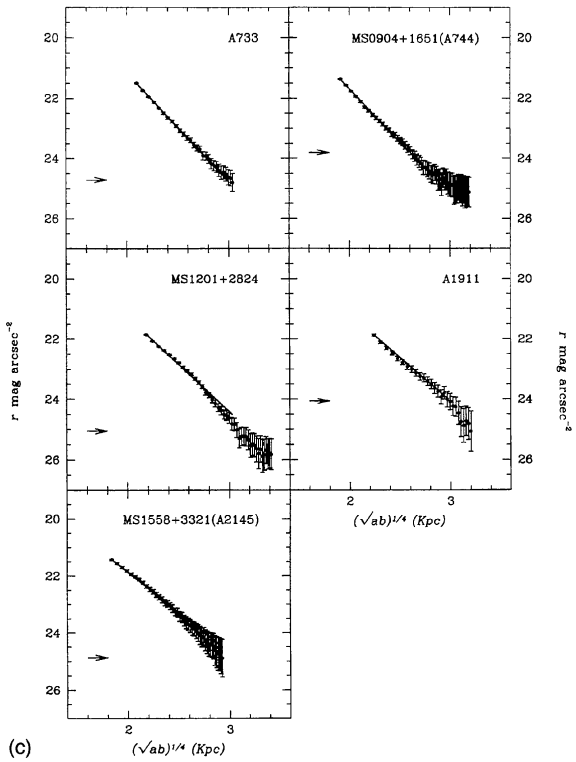

FIG. 2. BCM rest frame surface brightness profiles in the r filter plotted as a function of $r^{1/4}$, where $r=(ab)^{1/2}$. The continuous line is the best fitting de Vaucouleurs' law. The fit has been performed on every other data point beyond 2 times the FWHM of the seeing disc so that they can be considered independent, and within the radius where the observed galaxy surface brightness is 5 magnitudes fainter than the sky background (indicated by a horizontal arrow). Error bars are the composition of the counting statistics and of the sky background rms error. The profiles have been plotted outward as far as large and bright objects set in or the edge of the field of view is reached.

tistically significant excess outward of ~60 kpc. Figure 3(a) shows the residuals in the bi-dimensional image once a model galaxy with parameters equal to the best fitting de Vaucouleurs' is subtracted. As shown in the figure, this excess does not correspond to that of a classical halo, since it appears essentially along the major axis. Other peculiarity of this galaxy is the presence of a double nucleus as can be seen in Figure 3(b).

The analysis of the surface brightness profiles of our BCM sample shows that de Vaucouleurs' law provides an

TABLE 3. BCM parameters.

Cluster id	r_e kpc	μ_e r mag arcsec^{-2}	χ^2_{red}	$g-r$	$r-i$	M_r
MS0002+1556	$36.7^{+3.0}_{-1.1}$	$23.43^{+0.15}_{-0.10}$	0.17	0.35	0.29	−23.65
MS0013+1558	$24.6^{+1.0}_{-0.5}$	$22.71^{+0.05}_{-0.05}$	1.70[a]	0.39	0.28	−23.72
MS0037+2917 (A77)	$35.9^{+2.5}_{-3.1}$	$23.41^{+0.20}_{-0.15}$	1.04	0.37	0.27	−23.58
A84	$58.8^{+5.2}_{-2.9}$	$23.97^{+0.20}_{-0.05}$	0.16	0.34	0.29	−23.83
MS0102+3255	$18.1^{+1.7}_{-1.4}$	$22.59^{+0.50}_{-0.50}$	0.53	0.30	0.28	−23.28
A150	$39.3^{+3.1}_{-1.4}$	$23.47^{+0.15}_{-0.12}$	7.58[a]	0.26	0.33	−23.69
A180	$21.8^{+1.0}_{-1.9}$	$22.56^{+0.07}_{-0.19}$	0.12	0.29	0.30	−23.59
A279	$44.5^{+2.2}_{-0.8}$	$23.45^{+0.10}_{-0.05}$	0.16	0.20	0.35	−23.90
A399	$67.8^{+2.5}_{-3.0}$	$23.97^{+0.20}_{-0.10}$	0.67	0.20	0.27	−23.94
A401	$115.0^{+7.6}_{-4.8}$	$24.39^{+0.25}_{-0.07}$	0.04	0.42	0.24	−24.25
MS0301+1516	$21.1^{+1.1}_{-1.0}$	$23.09^{+0.06}_{-0.05}$	0.29	0.40	0.30	−22.99
A671	$42.4^{+3.1}_{-2.2}$	$23.29^{+0.35}_{-0.20}$	3.25[a]	0.33	0.13	−24.06
A733	$28.8^{+1.3}_{-2.1}$	$22.31^{+0.20}_{-0.35}$	0.32	0.21	0.18	−24.36
MS0904+1651 (A744)	$30.2^{+3.1}_{-2.2}$	$22.91^{+0.08}_{-0.10}$	0.81	0.21	0.29	−23.71
MS1201+2824	$48.4^{+2.1}_{-1.8}$	$23.28^{+0.10}_{-0.05}$	1.04	0.25	0.24	−24.10
A1911	$66.6^{+5.9}_{-2.3}$	$23.66^{+0.10}_{-0.15}$	0.48	0.29	0.23	−24.38
MS1558+3321 (A2145)	$75.5^{+9.4}_{-7.8}$	$24.56^{+0.40}_{-0.06}$	0.50	0.31	0.31	−23.62

[a]See text.

excellent description of the surface brightness profiles at radii between 10 and 45 kpc, where deviations are never greater than 0.05 mag. At larger radii, deviations generally remain of the order of the systematic errors, except in the case of A*150*, which has a rather complex morphology.

3.3 Color Profiles

$g-r$ and $r-i$ color profiles for all the BCMs have been computed from the surface brightness profiles in the three filters and are shown in Fig. 4. The method we employed to assess the presence of color gradients takes into account the effect of incorrect estimates of the sky background in one or both of the images (see Andreon *et al.* 1995 for a more detailed and complete explanation of the method). The solid lines in Fig. 4 represent the expected color profiles in the absence of color gradients. Vertical arrows indicate the position of superposed objects. Except in the case of A150, our plots are consistent with the absence of color gradients. This fact implies that color gradients are generally not a characteristic feature of BCMs, irrespective of the cluster selection criterion.

Let us now consider the $g-r$ radial profile of A150. The delicate point of the adopted method is that a normalization procedure is required. Whenever the data points scatter around the expected no–color–gradient line, the concept of a normalization radius becomes irrelevant since no color gradient would be meaningful regardless of the radius chosen. In the case of A150, if we normalize the expected value for the $g-r$ color profile at a radius smaller than that at which we found excess light with respect to the $r^{1/4}$ law, we would be led to state that the excess light is redder than that of the rest of the galaxy. On the other hand, if the expected color profile is normalized at a radius where the excess is present, the interpretation would be that the excess and the central region of A150 share the same $g-r$ color while at intermediate radii the galaxy is bluer. We have no reasons to prefer one of the two interpretations of this color profile; our data

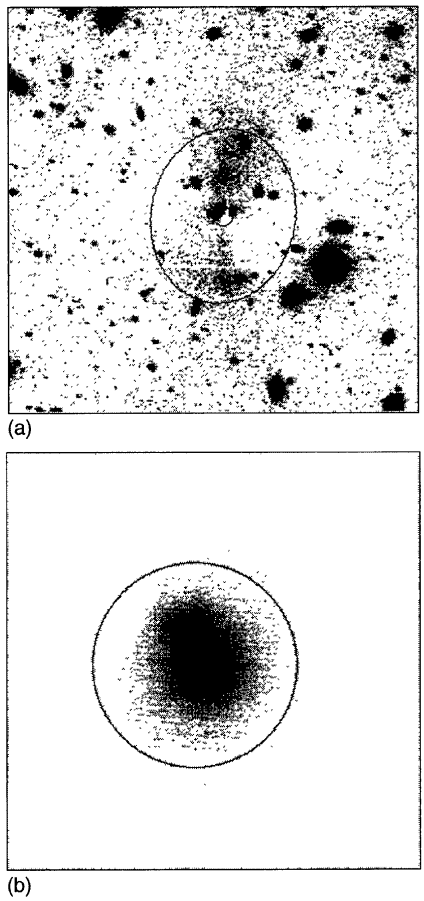

FIG. 3. (a) The residual image of A150 once a model galaxy with the best fitting de Vaucouleurs' parameters has been subtracted. The ellipse is the isophote at $(ab)^{1/2}=2r_e$ and the inner circle is two times the seeing disc. The excess surface brightness along the major axis is evident. (b) The A150 r image shows the presence of a resolved double nucleus. Again, the circle is two times the seeing disc.

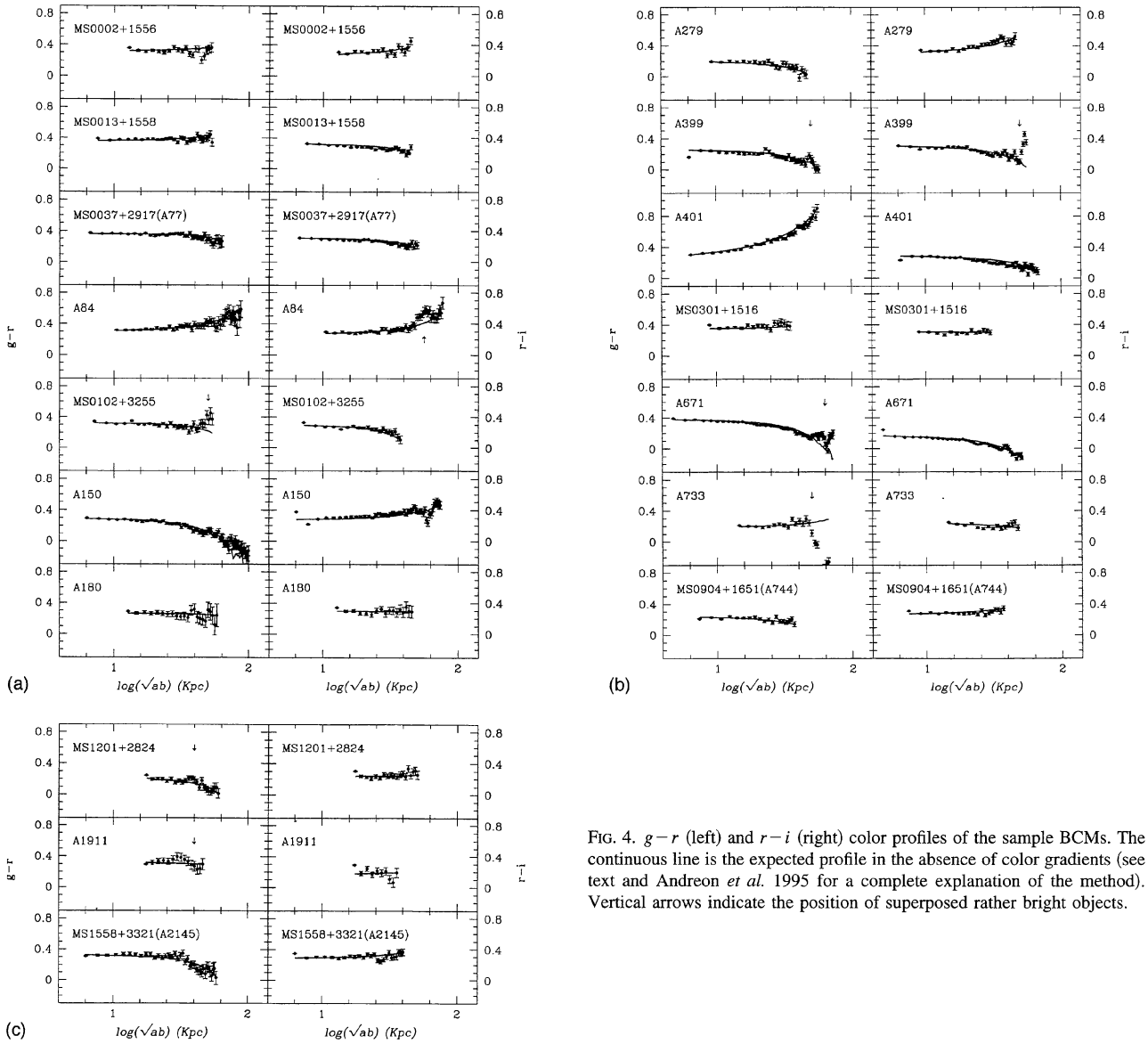

FIG. 4. $g-r$ (left) and $r-i$ (right) color profiles of the sample BCMs. The continuous line is the expected profile in the absence of color gradients (see text and Andreon *et al.* 1995 for a complete explanation of the method). Vertical arrows indicate the position of superposed rather bright objects.

do tell us, however, that A150 is the only BCM in the sample for which the $g-r$ color is not the same everywhere.

4. DISCUSSION

4.1 Comparison with Other Authors

Our sample includes seven galaxies which had been already studied by other authors: A150 and A401 were studied by Malumuth & Kirshner (1985) in the V filter, A671 is also in the Graham *et al.* (1996) sample observed in the Kron–Cousins R filter and MS0037+2917(A77), A279, A399, A401, A671 and A733 are also in the sample studied by Schneider *et al.* (1983b) and Hoessel & Schneider (1985) in the same Gunn r filter.

Figure 5 compares our profiles in the r band with those obtained by Malumuth & Kirshner (1985) for A150 and A401. In the case of A150, the agreement in surface brightness levels with Malumuth & Kirshner's data is excellent once the differences in filter bandpasses are taken into account. However, our fitting procedure yields a scale size ~30% smaller (and a correspondingly brighter effective surface brightness), probably because of the different range in radius over which the two fits are carried out. In the case of A401 we determined an effective radius ~25% larger than Malumuth & Kirshner. Porter *et al.* (1991) already compared the surface brightness profile they obtained for A401 with Malumuth & Kirshner's and showed that they derived a steeper profile and a higher surface brightness for the central regions. Our profile has a slope similar to that of Malumuth & Kirshner and also a value of the central surface brightness similar to that of Porter *et al.*'s. We should mention that the profile we derived for A671 is in very good agreement with Graham *et al.*'s (1996) as well as are the parameters obtained with the $r^{1/4}$ law.

For the other commonly studied BCMs, a comparison with Hoessel & Schneider's (1985) results shows differences in the effective radii of the order of 7″ to 10″. Several causes could explain these differences: the way seeing effects are

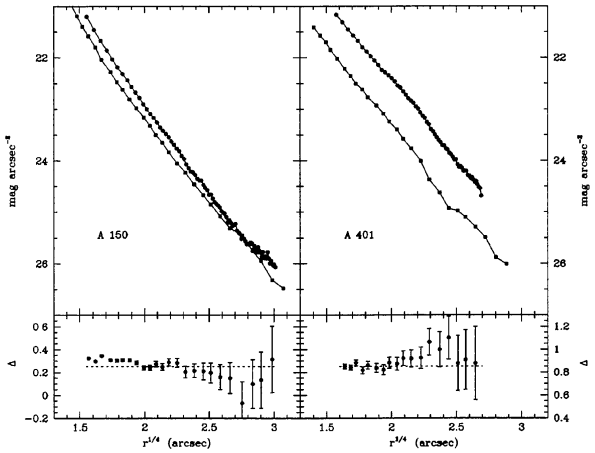

FIG. 5. Comparison of our r band surface brightness profiles of A150 and A401 (upper panels, full dots) with the V band profiles of Malumuth & Kirshner (1985) (upper panels, open squares). The lower panels show the difference between the profiles we obtained and those obtained by Malumuth & Kirshner. Our data points (and errors) have been resampled at the same radii as Malumuth & Kirshner's data.

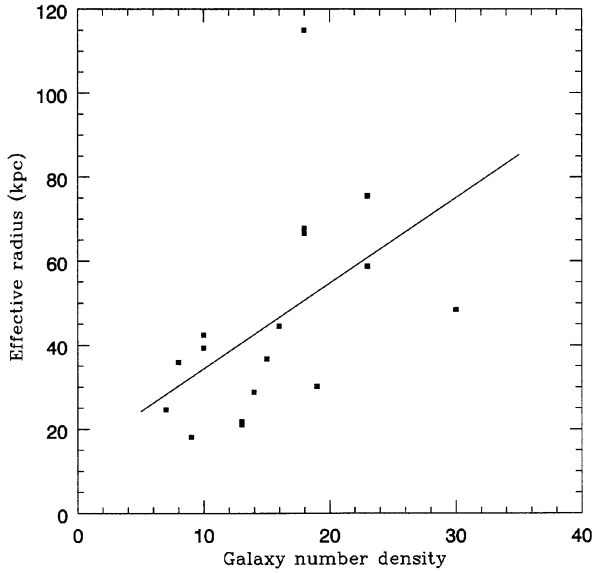

FIG. 6. Effective radius r_e vs the number of galaxies brighter than $M_r=-18$ within a 200 kpc radius from the center of the BCM. The continuous line is the least-squares fit through the data points, yielding a correlation coefficient $r=0.50$.

taken into account, the outermost radius to which the fit is applied, the way eccentricity is taken into account. However, the relation between effective radius and surface brightness of BCMs found by Hoessel & Schneider (1985) is also a very good fit to the whole of our data. We conclude that a detailed, object–to–object comparison is rather meaningless because it depends on the data quality, and on the reduction and analysis techniques adopted. However, the statistical properties of the samples are much more robust and reproducible regardless of the authors; therefore these are really representative of the samples.

4.2 Intrinsic Colors

In Table 3, columns 5 and 6 give the rest–frame $g-r$ and $r-i$ colors, and column 7 the absolute magnitude M_r, all computed within a radius $r=\sqrt{ab}=38$ kpc.

The average rest–frame $r-i$ color of the BCMs in our sample is $\langle r-i\rangle=0.28$ with a sample standard deviation of 0.05. This value agrees with the one given by Schneider *et al.* (1983a) and the dispersion around the mean is of the same order as the photometric accuracy obtained for this color (Gar96). In this case the mean and the median values do coincide.

The average rest–frame $g-r$ color is $\langle g-r\rangle=0.31$ with a sample standard deviation of 0.09. Once the shift in the g filter of our photometric system with respect to that of Schneider *et al.* (1983a) (Gar96) is taken into account, also this value is compatible with the BCM rest–frame colors of those authors. The standard deviation is however about a factor of 2 higher than expected on the basis of the photometric errors. If we use the k–corrections given by Frei & Gunn (1994) for E galaxies, all galaxies have slightly redder rest–frame colors with an average $\langle g-r\rangle=0.35$ and a sample standard deviation of 0.07. Although the standard deviation remains higher than expected, it seems difficult to claim that BCMs show an intrinsic dispersion in this color. We recall that also in Andreon *et al.*'s (1995) BCM sample, no intrinsic dispersion in the $B-V$ color was found.

4.3 Relation with the Environment

Andreon *et al.* (1995) showed that a correlation existed between the BCM effective radius and the cluster richness. In that paper, Abell's richness class was used as a measure of the environment galaxy density. For the present sample, we cannot use Abell richness class as this is not available for the X-ray selected clusters. However, we can correlate BCM effective radii with the local galaxy density. The cluster complete catalogs of Gar96 allow us to count galaxies brighter than $M_r=-18$ in circles of projected radii equal to 200 kpc at the cluster redshift and centered on the BCM itself. Plotted against the effective radius (Fig. 6), this measure of the local galaxy density confirms and quantifies the result of Andreon *et al.* (1995). Shallower BCMs are found in environments, which, at the present epoch, are locally denser.

4.4 BCMs as Standard Candles: The Tolman (1930) Test

Sandage & Perelmuter (1990) suggest that BCMs can be used to test whether the Universe is expanding or not. To check the cosmological dimming, they looked for a redshift dependence of the galaxy surface brightness at a fixed metric radius.

For the galaxies studied by Sandage & Perelmuter (1990), the observed scatter in the relation between $\log(1+z)$ and μ, i.e., the scatter in the cosmological dimming, once the Malmquist bias (Malmquist 1920) is removed (see Sandage & Perelmuter 1990 for details), is ~ 0.25 mag arcsec^{-2}. For our BCM sample, in the range $0.05<z<0.2$, we find a corresponding scatter of 0.22 mag arcsec^{-2}. The slope of the linear regression between $\log(1+z)$ and μ, before Malmquist corrections, is 3 times larger than the Tolman signal for Sandage & Perelmuter's (1990) samples, yet for our sample

is of the same amplitude as the Tolman signal. This suggests that our sample is only slightly affected by the Malmquist bias. This fact is probably due to the different sample compositions, and, most probably, to the fact that in our sample about half of the BCMs are there because they are members of clusters serendipitously detected in an X-ray survey. Although the cluster X-ray luminosity is correlated with the BCM absolute magnitude (Valentijn & Bijleveld 1983), their surface brightness at a fixed metric radius is only weakly dependent on it, implying that through X-ray selection the amount of bias introduced on the quantity to test as redshift increases is quite small. We suggest that the Tolman test could give significant results if carried out on a proper sized sample of BCMs drawn from purely X-ray selected clusters. Unfortunately, the number of BCMs in X-ray selected clusters in our sample is still too small and extends to relatively low redshift values for the Tolman test to be successful.

5. CONCLUSIONS

The multicolor surface brightness photometry of this mixed sample of 17 BCMs with redshifts extending to $z\sim0.2$ shows that:

- The surface brightness profile of these BCMs is generally well described by de Vaucouleurs' law out to radii of $\sim60-80$ kpc. Structural peculiarities such as changes in isophotal position angle and/or ellipticity are largely absent in our sample.
- Although normal and small size ellipticals do show color gradients (Sparks & Jørgensen 1993), these gradients are a rather rare feature in BCMs. The only color gradient detected in our sample corresponds to A150. This galaxy also shows a brightness excess with respect to the $r^{1/4}$ law along the major axis and a double nucleus. Andreon *et al.* (1995), who analyzed color profiles in the same way as we did, found that 2 BCMs in a sample of 9 show gradients in the $V-i$ color (and 2 out of 8 BCMs in the $B-V$ color). We could thus infer that $\sim10\%$ of BCMs presents measurable color gradients in broad–bandpasses redwards of the 4000 Å break.
- BCM $g-r$ and $r-i$ colors (integrated within 38 kpc radius) do not show any intrinsic dispersion. If an intrinsic dispersion is present in the bluer color, this is of the same order as the uncertainties in the k–corrections.

This *normality* of BCMs which tends to assimilate them to the more general class of elliptical galaxies does not remove their main peculiarity: the large scale size of many of them (about half of the BCMs we studied have effective radii $r_e>40$ kpc). Galaxies so large and bright ($M_r<-24$) are found only in clusters of galaxies. Furthermore, we have shown that their linear dimensions scale with the local galaxy density as determined at the present epoch. The sizes do not seem to be related either to the cluster morphology, or to the way clusters are selected. Bautz–Morgan type I clusters possess BCMs among the less extended (A180, with an effective radius of only 22 kpc) and among the most extended ones in our sample (A401, $r_e=115$ kpc). It is true that only one of the five X-ray selected clusters (i.e., clusters which have been missed in the Abell catalog) has a BCM with an effective radius larger than 40 kpc (MS1201+2824, $r_e=48$ kpc), but this is naturally explained by a selection effect: these clusters are not found in the Abell catalog because they are not very rich, and therefore their BCMs are not very extended. Nor is the X-ray luminosity of the clusters correlated with the size of the BCM galaxy.

Merging is considered the most likely mechanism for the formation of these giant galaxies. It also provides a way to dilute any color gradients (White 1980) (which we do not generally observe). Two different cD formation scenarios have been investigated: either cDs are the product of repeated mergers after cluster virialization (Malumuth 1992; Bode *et al.* 1994), or the merging events leading to the cD formation occurred before or during cluster formation (Merritt 1988). There is evidence of merging events occurring in clusters at the present epoch, as shown by the peculiar E galaxy IC 1182 in the Hercules cluster which is the result of a recent interaction between an elliptical and a spiral galaxy (Tarenghi & Maccagni, private communication). Generally, simulations consider the luminosity of the merger products and, if this is a few times L^*, the resulting galaxy is identified as a cD, i.e., the most luminous galaxy at the center of the cluster. Dynamical arguments lead us to consider the cluster as a whole, that is to say, the entire cluster galaxy population comes into play, mainly since it is largely concentrated within the core radius. Furthermore, it is sometimes assumed that the large extent of the cD galaxy is mainly due to the presence of a halo. The relation we found is between *de Vaucouleurs effective radius and the galaxy number density within a 200 kpc radius from the BCM itself.* It is therefore a relation between a quantity which measures the slope of the surface brightness profile, independently of the presence of an extended halo (which does not seem to be a common feature in our sample), and a quantity which measures the density of the environment as it is now. Both quantities are presumably the end points of evolutionary processes, which might not necessarily occur with the same time scales. The implications of Malumuth's (1992) simulations for cDs, provided the dynamical friction in the real universe is as efficient as in his code, are, among others, that cDs are a relatively recent phenomenon or that they are not formed in their present environment. Our data would tend to exclude this last possibility, and, because of the generally dull appearance, do probably suggest that some time has elapsed since the last dramatic event. This seems to be in contrast with the high peculiar velocities sometimes shown by cDs (Hill *et al.* 1988; Sharples *et al.* 1988; Zabludoff *et al.* 1990; Malumuth *et al.* 1992). However, substructure is a common feature of many clusters (Geller & Beers 1982; Jones & Forman 1984; Bird 1994), and when it is taken into account in the dynamical analysis of the clusters, the peculiar velocities of the central galaxies tend to disappear (Bird 1994). Our data thus seem to suggest that the growth in size of the BCMs is governed by the *local* environment and that, in many cases, the dominant galaxy and the concentration of galaxies surrounding it represent, at least for a non negligible amount of time, a dynamical entity with respect to the whole cluster. It would be extremely interesting to probe the dy-

namical status of this sample with respect to the very local and to the overall cluster environment since this would be a powerful diagnostic tool for the formation scenarios.

The authors warmly acknowledge the support of the OAN staff both in San Pedro Martir and Ensenada. The Time Allocation Committee of the UNAM–OAN is thanked for the generous allocation of telescope time. S.A. acknowledges the award of a CNR fellowship. We are grateful to the referee, E.M. Malumuth, for his useful suggestions which have helped us to improve the contents and presentation of the paper.

REFERENCES

Abell, G. O., Corwin, H. G., & Olowin, R. P. 1989, ApJS, 70, 1
Andreon, S., Garilli, B., Maccagni, D., Gregorini, L., & Vettolani, G. 1992, A&A, 266, 139
Andreon, S., Garilli, B., & Maccagni, D. 1995, A&A, 300, 711
Bautz, L. P., & Morgan, W. W. 1970, ApJ, 162, L149
Bird, C. M. 1994, AJ, 107, 1637
Bode, P. W., Berrington, R. C., Cohn, H. N., & Lugger, P. M. 1994, ApJ, 433, 479
Caon, N., Capaccioli, M., & D'Onofrio, M. 1993, MNRAS, 265, 1013
de Vaucouleurs, G. 1948, Ann. d'Ap., 11, 247
Frei, Z., & Gunn, J. E. 1994, AJ, 108, 1476
Garilli, B., Bottini, D., Maccagni, D., Carrasco, L., & Recillas, E. 1996, ApJS, 105, 191(Gar96)
Geller, M., & Beers, T. C. 1982, PASP, 94, 421
Gioia, I., *et al.* 1990, ApJS, 72, 567
Graham, A., Lauer, T. D., Colless, M., & Postman, M. 1996, ApJ, 465, 534
Hill, J. M., Hintzen, P., Oegerle, W. R., Romanishin, W., Lesser, M. P., Eisenhamer, J. D., & Batuski, D. J. 1988, ApJ, 332, L23
Hoessel, J., & Schneider, D. 1985, AJ, 90, 1648
Jones, C., & Forman, W. 1984, ApJ, 276, 38
Malmquist, G. 1920, Lund Medd, Ser II, No. 22
Malumuth, E. M. 1992, ApJ, 386, 420
Malumuth, E. M., Kriss, G. A., Dixon, W. V. D., Ferguson, H. C., & Ritchie, C. 1992, AJ, 104, 495
Malumuth, E. M., & Kirshner, R. P. 1985, ApJ, 291, 8
Merritt, D. 1988, in The Minnesota Lectures on Clusters of Galaxies and Large-Scale Structure, edited by J. M. Dickey (Brigham Young University Press, Provo), p. 175
Porter, A. C., Schneider, D. P., & Hoessel, J. G. 1991, AJ, 101, 1561
Sandage, A., & Perelmuter, J. 1990, ApJ, 370, 455
Schneider, D. P., Gunn, J. E., & Hoessel, J. G. 1983a, ApJ, 264, 337
Schneider, D. P., Gunn, J. E., & Hoessel, J. G. 1983b, ApJ, 268, 476
Sersic, J.-L. 1968, Atlas de Galaxies Australes (Obs. Astronomico, Cordoba)
Sharples, R., Ellis, R., & Gray, P. 1988, MNRAS, 231, 479
Sparks, W., & Jørgensen, I. 1993, AJ, 105, 1753
Stark, A. A., *et al.* 1992, ApJS, 79, 77
Tolman, R. C. 1930, Proc. Natl. Acad. Sci. USA, 16, 511
Valentijn, E. A., & Bijleveld, W. 1983, A&A, 125, 223
White, S. 1980, MNRAS, 191, 1P
Zabludoff, A. I., Huchra, J. P., & Geller, M. J. 1990, ApJS, 74, 1